Effects of Nanostructure on Catalytic Degradation of Ethanol on $SrCO_3$ Catalysts

Li Wang and Yongfa Zhu*

Key Lab of Organic Optoelectronics and Molecular Engineering, Beijing 100084, People's Republic of China, and Department of Chemistry, Tsinghua University, Beijing 100084, People's Republic of China

Received: September 12, 2004; In Final Form: November 25, 2004

Degradation of ethanol over $SrCO_3$ nanowires and nanoparticles was used as a model reaction to investigate the effect of nanostructure on chemical property. Differences in catalytic degradation activity with nanostructure are evaluated. The results indicated that catalytic activity of $SrCO_3$ particles increases with decreasing of particle size due to high surface area. But this conclusion cannot be applicable to evaluating $SrCO_3$ nanowires and nanoparticles. $SrCO_3$ nanowires have lower ignition temperatures and wider working temperature ranges than $SrCO_3$ nanoparticles, though nanowires had lower surface areas. Besides, ethanol degraded over nanowires in three ways, and the dominating reaction changes with reaction temperature. Consequently, the main degradation products of nanowires differed with temperature. But for nanoparticles, acetaldehyde is the only main product. Since transmission electron microscopy, X-ray diffraction, and bond equilibrium theory analysis demonstrated that nanowires and nanoparticles had similar crystal structure, surface area, and grain size, the differences in catalytic degradation activity between $SrCO_3$ nanowires and nanoparticles can be attributed to different distributions of active sites, as proven by CO_2 and ethanol temperature programmed desorption.

1. Introduction

Nanosized materials have attracted widespread attention for their special features that differ from bulk materials since the 1990s. Catalysts and chemical sensors based on nanosized materials have been developed rapidly. For example, ABO_3 type perovskite oxide composites and noble metal supported oxides with nanostructure are widely used in catalytic combustion of volatile organic compounds,[1] greenhouse gases,[2] methane,[3] and so on. The individual semiconducting single-walled carbon nanotube (SWNT)-based chemical sensors that are capable of detecting small concentrations of gas molecules have been realized,[4] boron-doped silicon nanowire nanosensors have showed highly sensitive and selective detection of biological and chemical species,[5] and palladium mesowire arrays for detection of hydrogen have been described based upon resistivity changes caused by the changes in the structure of the wire itself.[6] It is well-known that nanostructure generally has great effect on properties of nanomaterials,[7] but few investigations in this field are focused on variation of chemical property with nanostructure. Catalysts are one of the important applications for many nanomaterials. Since a catalytic reaction generally occurs at a surface and it strongly depends on the distribution of the active site, which is greatly effected by structure, investigation on the relationship between nanostructure and catalytic activity has valuable importance.

Here, we report the significant effect of nanostructure on oxidation activity of $SrCO_3$ nanomaterials. On the basis of the work reported by Zhang et al.,[8] in which $SrCO_3$ was proven to be a potential chemical sensor, catalytic degradation of ethanol was used as the model reaction. The results indicated that compared with a $SrCO_3$ nanoparticle, though $SrCO_3$ nanowire had the same crystal structure, similar grain size, and lower surface-to-volume ratio, the nanowire had higher catalytic activity. Further investigation on CO_2 and ethanol temperature programmed desorption (TPD) proved that the variation of catalytic activity with nanostructure could be attributed to different distribution of catalytic active sites.

2. Experimental Section

2.1. Preparation and Characterization of $SrCO_3$ Nanowires and Nanoparticles. $SrCO_3$ nanowires were prepared by reacting a $Sr(OH)_2$ solution with CO_2 in air.[9] Fresh saturated $Sr(OH)_2$ solution absorbed CO_2 in air for 1 h and then was dried at 60 °C for 4 h to form $SrCO_3$ nanowires, and then the product was washed with distilled water and dried at 60 °C.

$SrCO_3$ nanoparticles were prepared by the rapid precipitation method. After 0.1 M Na_2CO_3 solution was dropped into 0.1 M $SrCl_2$ solution while being stirred by a magnetic stirrer, white deposition formed. The deposition was stirred for 10 h to prepare 40 nm particles and 24 h to prepare 80 nm particles. And then the obtained $SrCO_3$ nanoparticles were washed with distilled water 3−5 times and dried at 60 °C. Commercial $SrCO_3$ was used as bulk material to evaluate the catalytic activity of nanomaterials. It was analytical reagent grade with a purity of greater than 99.0%.

The particle size of $SrCO_3$ materials were measured using transmission electron microscopy (TEM, Hitachi H-800) with a 200 kV accelerating voltage for the electron beam. Their crystal structure was measured by X-ray powder diffraction (XRD) on a Rigaku DMAX-2400 with Cu Kα radiation. Before CO_2-TPD and ethanol-TPD analyses, about 0.1 g of catalyst was first heated at 350 °C for 2 h in flowing He gas to remove contaminations adsorbed on the surface, then saturated with CO_2 or ethanol at room temperature for 1 h. Mass spectroscopy was used as a detector in TPD analysis.

2.2 Evaluation of Catalytic Oxidation Properties of $SrCO_3$ Nanowires and Nanoparticles. Evaluation of catalytic oxidation properties was carried out in a thermal reactor along with a gas chromatography (GC) detector. As shown in Figure 1,

* Author to whom correspondent should be addressed. Phone: (+8610)-62783586. Fax: (+8610)-62787601. E-mail: zhuyf@chem.tsinghua.edu.cn.

10.1021/jp045884d CCC: $30.25
Published on Web 03/01/2005

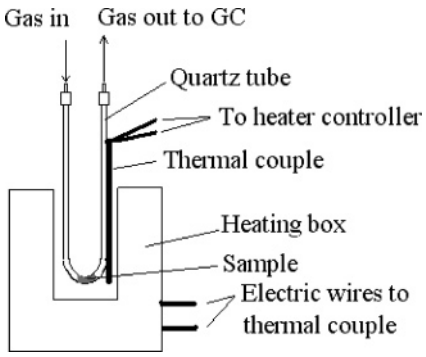

Figure 1. Schematic diagram of the thermal reactor.

0.1 g of $SrCO_3$ powder was put into an U-shaped quartz tube, which was 10 mm in diameter, and 1 g of quartz powder covered the $SrCO_3$ catalyst at the end of the tube to prevent the catalyst from washing away by the flow. Thermal catalytic oxidations at different temperatures were realized with an oven, which was controlled by a heater controller and a thermal couple. Air and ethanol vapor were accurately mixed by a mass flow meter, and the flow rate was examined by a bubble flow meter. The concentration of ethanol was determined by GC, with a GDX-403 GC-column (1.5 mm × 4 mm, 373 K) and hydrogen flame detector.

3. Results and Discussion

3.1 Characterization of $SrCO_3$ Nanowires and Nanoparticles. Figure 2 showed the TEM photographs of $SrCO_3$ nanowires and nanoparticles. All of these $SrCO_3$ nanomaterials are well-dispersed, and their morphology and grain size can be easily evaluated. $SrCO_3$ nanowires were uniform, and their average diameter and length were about 30 nm and 2.5 μm, respectively, as shown in Figure 2A. These nanowires are rough, but no particle boundaries can be clearly found in every nanowire, indicating that the nanowires are continuous and holistic. In addition, the electron diffraction in the upper-left corner showed that only (001) appeared along the length direction of nanowires, indicating that the $SrCO_3$ nanowires were crystalline and grown preferentially along the *c*-axis.[9,10] In Figures 2B and 2D, $SrCO_3$ particles are not very uniform, and their average grain sizes were about 40 and 80 nm, respectively. Electron diffraction patterns of both nanoparticle samples indicated that the nanoparticles were all crystalline, as shown by the typical electron diffraction in the upper-right corner of Figure 2B. Figure 2D shows the TEM micrograph of commercial $SrCO_3$. It showed that these particles were not uniform with an average particles size of about 250 nm. Similar to 40 and 80 nm particles, electron diffraction analysis showed that every particle was a single crystal.

The X-ray diffraction (XRD) patterns of nanowires and nanoparticles were similar both in peak position and in relative intensity, indicating that nanowires and nanoparticles had the same crystal structure. According to the Joint Committee on Powder Diffraction Standards (JCPDS 84-1778), these nanostructured materials were both orthorhombic $SrCO_3$. Besides, from the broadened diffraction peaks of nanowires, 40 nm nanoparticles, and 80 nm nanoparticles, it can be concluded that the crystal sizes are 40 nm nanoparticles < nanowires < 80 nm nanoparticles, according to the Scherrer equation.[11]

In addition, the specific surface areas of $SrCO_3$ nanowires, 80 nm nanoparticles, and 40 nm nanoparticles were about 22, 16, and 42 m^2/g, respectively, as determined by using bond equilibrium theory (BET) analysis. This result implied that the grain size of the nanowires may be larger than 40 nm but less than 80 nm.

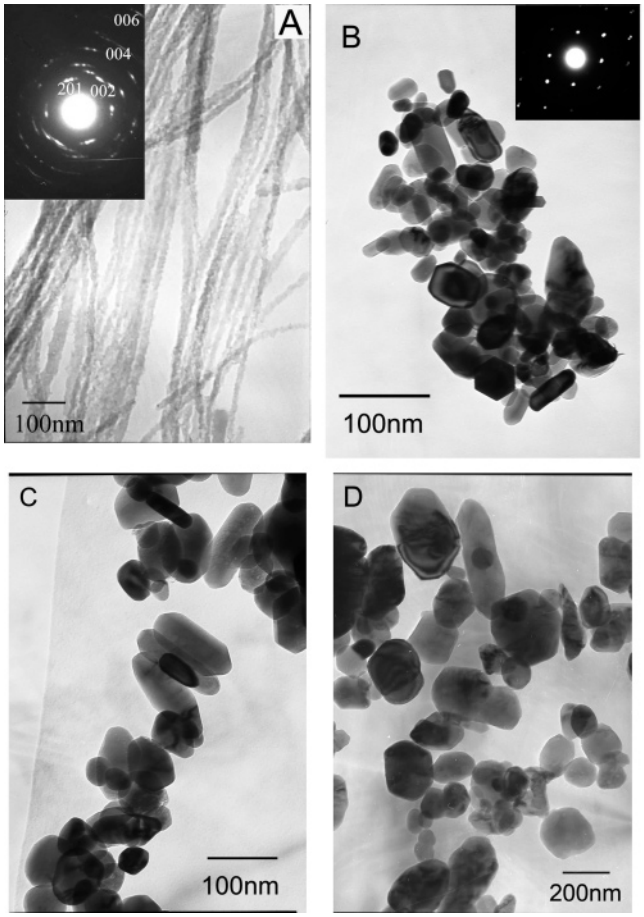

Figure 2. TEM photographs of the $SrCO_3$ catalyst. (A) $SrCO_3$ nanowires; (B) 40 nm $SrCO_3$ nanoparticles; (C) 80 nm $SrCO_3$ nanoparticles; (D) 250 nm commercial $SrCO_3$ nanoparticles.

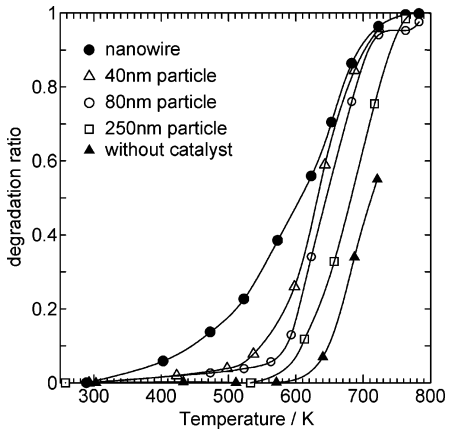

Figure 3. Variation of ethanol degradation ratio over $SrCO_3$ nanowires and nanoparticles with reaction temperature. Ethanol concentration = 10 000 ppm; O_2 = 20%; flow rate = 80 mL/min.

3.2. Catalytic Oxidation of Ethanol by $SrCO_3$ Nanowires and Nanoparticles. *3.2.1. Effect of Temperature on Ethanol Degradation over $SrCO_3$ Nanowires and Nanoparticles.* Variations of the ethanol degradation ratio over different $SrCO_3$ nanomaterials with temperature were shown in Figure 3. Three conclusions can be drawn from this result. First, $SrCO_3$ nanomaterials can greatly lower the degradation temperature of ethanol. This result is consistent with reported work, in which it was demonstrated that $SrCO_3$ material showed good catalytic

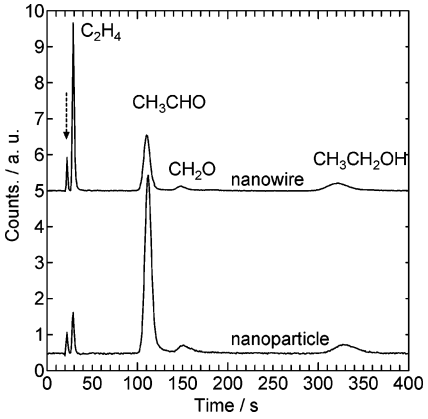

Figure 4. GC chromatograms of the oxidation products of ethanol on $SrCO_3$ nanowires and nanoparticles at 673 K. Ethanol concentration = 10 000 ppm; O_2 = 20%; flow rate = 80 mL/min.

activity due to its basicity.[8,12] The ignition temperature of ethanol was decreased by approximately 150 °C for nanoparticles, and it decreased by approximately 270 °C for nanowires. Second, the catalytic activity of nanoparticles increased with decreasing particle size. As shown in Figure 3, 40 nm particles exhibited slightly higher degradation ability than that of 80 nm particles in all working temperature ranges, and 80 nm particles showed obviously higher catalytic activity than that of 250 nm particles. Since nanoparticles were similar in morphology and crystal structure, the weak advantage of 40 nm nanoparticles can be attributed to their higher surface area. The third conclusion seemed contrary with the second conclusion. Though nanowire catalysts had lower surface areas than nanoparticles with a particle size of 40 nm, nanowire catalytic activity was significantly higher. For example, the nanowire ignition temperature was about 120 °C lower than that of the nanoparticle, and the degradation ratio was observably higher at temperatures below 650 K. In comparison with nanoparticles, nanowires preferentially grew in a certain direction. Therefore, this remarkable difference between nanowires and nanoparticles may be related with their nanostructures, which generally determined the distribution of the active sites.

However, though three catalysts showed different catalytic activities, they had almost the same total conversion temperature. This result indicated that nanowires had a wider working temperature range. Is the degraded ethanol all totally oxidized, and how does nanostructure affect ethanol catalytic oxidation? Further investigation was undertaken, and 40 nm nanoparticles and nanowires were chosen as the model system.

3.2.2. Effects of Temperature on Products of $SrCO_3$ Nanowires and Nanoparticles. A typical chromatogram of the gas catalyzed by $SrCO_3$ nanowires and 40 nm particles at 673 K is shown in Figure 4. A temperature of 673 K was chosen to illustrate the reaction products, since the degradation ratios of the two catalysts were both near 80% at this temperature. Except ethanol, C_2H_4, CH_3CHO, and CH_2O can be observed as degradation products, implying that ethanol was catalyzed in different manner on these two $SrCO_3$ nanomaterials. In addition, the three products showed different yields over each catalyst. For $SrCO_3$ nanoparticles, CH_3CHO was obviously the main product. But for $SrCO_3$ nanowires, C_2H_4 increased greatly, and CH_3CHO decreased in the products. This result indicated that different reactions dominated the degradation of ethanol over nanowires and nanoparticles, respectively, even under the same conditions.

Formation of CH_3CHO, CH_2O, and C_2H_4 over $SrCO_3$ nanowires and nanoparticles with different temperatures are shown in Figure 5. The working conditions were ethanol concentration = 10 000 ppm, O_2 = 20%, and flow rate = 80 mL/min.

Figure 5A showed the variation of CH_3CHO formation with temperature over $SrCO_3$ nanowires and nanoparticles. It can be shown from this figure that CH_3CHO formed throughout the working temperature range, and it showed a peak distribution at about 670 K on both $SrCO_3$ catalysts, but its yield was different over the two catalysts. For example, the maximal yield of the nanoparticle was about 2.5 times of that of the nanowire. According to Figure 3, CH_3CHO formed from ignition temperature and decreased greatly when the degradation ratio was above 90%. In addition, these two curves were similar to the degradation ratio curve at temperatures under 600 K. This can be explained by the fact that $CH_3CH_2OH \rightarrow CH_3CHO$ dominated ethanol conversion at low temperatures and CH_3CHO was also degraded at high temperature.

Figure 5B shows the comparison of CH_2O formation with temperature on nanowires and nanoparticles. Both of the curves showed peak distributions, and they reached the maximal values around 550 and 610 K on nanowires and nanoparticles, respectively. Furthermore, the maximum yield over the nanowires was 4 times higher than that over the nanoparticles. According to Figure 3, all of the above indicated that CH_2O was mainly formed at low temperatures and that the degradation ratio of ethanol was only about 20%.

Figure 5D showed the variation of C_2H_4 formation with temperature over nanowires and nanoparticles. Similar to the formation of CH_2O, the maximal yield of C_2H_4 on nanowires was 9 times higher than that on nanoparticles. But C_2H_4 could be observed only when the temperature was higher than 525 and 620 K for nanowires and nanoparticles, respectively. Though the temperatures corresponding to the maximal yields were different for the two catalysts, they were all approximately total conversion temperature, indicating that C_2H_4 was mainly formed at high temperatures at which ethanol was totally degraded.

It can be concluded from Figures 5A−C that the three products had different formation temperatures. For the $SrCO_3$ nanowire catalyst, the main product changed with temperature. At low temperature, CH_3CHO and CH_2O formed with approximate yield, but CH_3CHO increased greatly and became the only main product with the temperature rising. When the temperature was greater than 730 K, C_2H_4 emerged and became the main product. However, CH_3CHO was the only main product all through the working temperature range for the $SrCO_3$ nanoparticles.

Since various products in a catalytic reaction are generally related to different catalytic active sites, the variation of CH_3CHO, CH_2O, and C_2H_4 formation with temperature can be attributed to different distributions of three kinds of catalytic active centers on $SrCO_3$ nanowires and nanoparticles. Further investigations on catalytic active sites were performed using TPD, which will be discussed below.

3.2.3. Effects of Flow Rate on Catalytic Oxidation of Ethanol over $SrCO_3$ Nanowires and Nanoparticles. Effects of flow rate on the catalytic degradation of ethanol over $SrCO_3$ nanowires and nanoparticles was investigated, as shown in Figures 6A and 6B, respectively. A temperature of 623 K was chosen as the working temperature, since the degradation ratio of both catalysts was near 50% (the degradation ratio was about 55% for nanowires and 45% for nanoparticles) at this temperature and the degradation reaction may be easily affected by changes in the reaction condition. It can be observed that for ethanol degradation little changed with the flow rate over the nanowires.

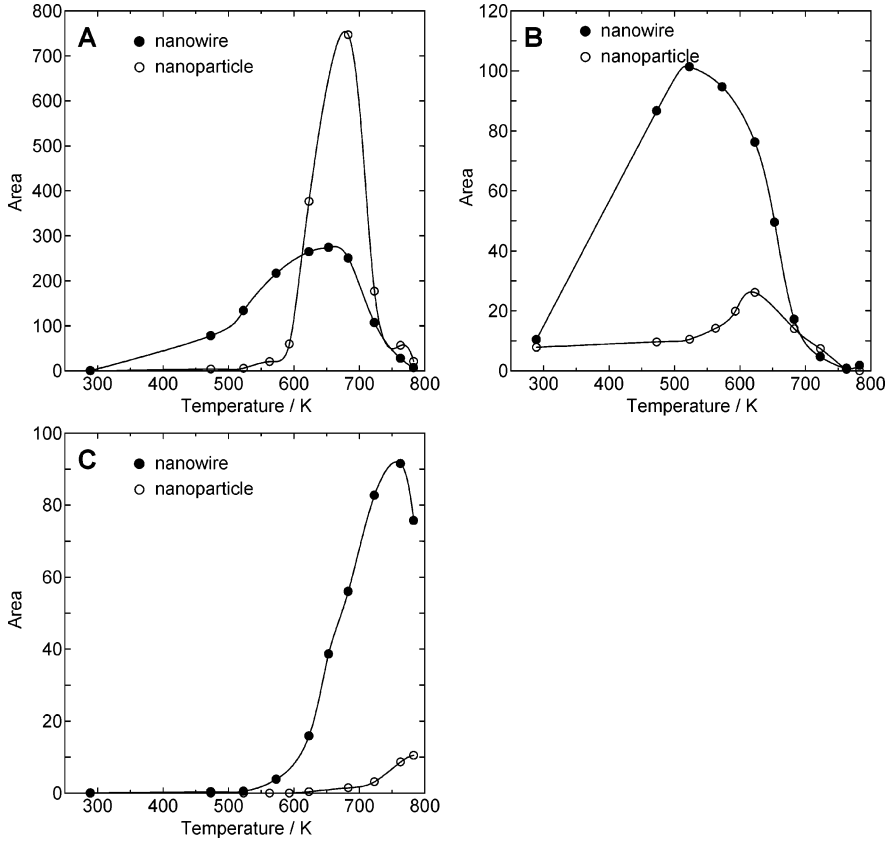

Figure 5. Formation of (A) CH_3CHO, (B) CH_2O, and (C) C_2H_4 on $SrCO_3$ nanowires and nanoparticles with reaction temperature. Ethanol concentration = 10 000 ppm; O_2 = 20%; flow rate = 80 mL/min.

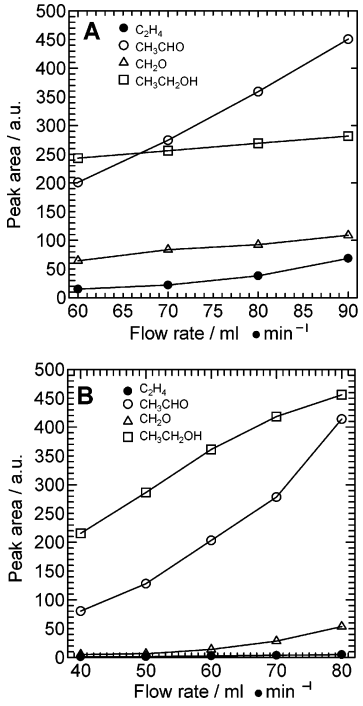

Figure 6. Effect of flow rate on every species in ethanol oxidation at 623 K over (A) $SrCO_3$ nanowires and (B) $SrCO_3$ nanoparticles.

For example, the peak area of ethanol increased by only 20 for nanowires but 100 for nanoparticles when the flow rate decreased from 60 to 80 mL/min. This was because the catalytic activity of the nanowires is about 2 times higher than that of the nanoparticles, as shown in Figure 3.

Another phenomenon that can be observed was that the oxidation products and residual reactant all increased with the flow rate for both catalysts, but CH_3CHO increased the most sharply. For nanowires, CH_3CHO increase 1.25 times, but the reactant increased only 0.12 times. This can be explained as follows. Besides being mainly degraded into C_2H_4, CH_2O, and CH_3CHO, part of the ethanol was totally converted into CO_2 and H_2O, which cannot be detected by a hydrogen flame detector but has been proven by mass spectroscopy. In ethanol degradation, $CH_3CH_2OH \rightarrow CH_3CHO$ was the main conversion, and other products were produced by further oxidation of CH_3CHO.[13] Fast flow greatly reduced degradation of CH_3CHO, so more CH_3CHO was formed, but less was consumed, causing a faster increase than ethanol.

3.2.4. Effects of Ethanol Concentration on Catalytic Oxidation of Ethanol over $SrCO_3$ Nanowires and Nanoparticles. The effects of concentration on ethanol oxidation over $SrCO_3$ nanowires and nanoparticles were investigated, as shown in Figures 7A and 7B. It was observed that all substances increased with concentration to a different extent. For example, products increased more than ethanol in Figure 7A, while they increased less than ethanol in Figure 7B. This indicated that ethanol concentration had weak effect on degradation over nanowires but a great effect over nanoparticles, demonstrating that nanowires had a higher catalytic activity, which was in agreement with the result shown in Figure 3.

In Figure 7A, CH_2O increased flatly, but C_2H_4 and CH_3CHO increased sharply with concentration, indicating that C_2H_4 and CH_3CHO were the main products at this temperature. This results were consistent with those shown in Figure 5. However, in Figure 7B, the phenomena are different. Both ethanol and CH_3CHO increase greatly with concentration, while C_2H_4 and CH_2O showed weak changes with concentration, implying that CH_3CHO is the main product no matter whether oxidation proceeded completely or not.

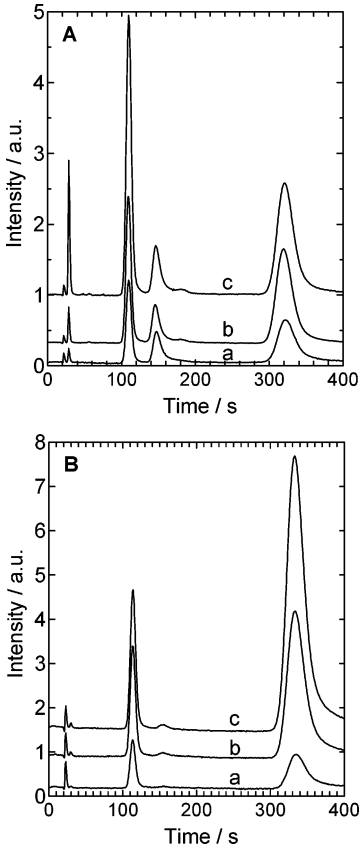

Figure 7. Effect of concentration on ethanol oxidation over (A) $SrCO_3$ nanowires and (B) $SrCO_3$ nanoparticles at 623 K. a = 10 000 ppm; b = 13 000 ppm; c = 16 000 ppm.

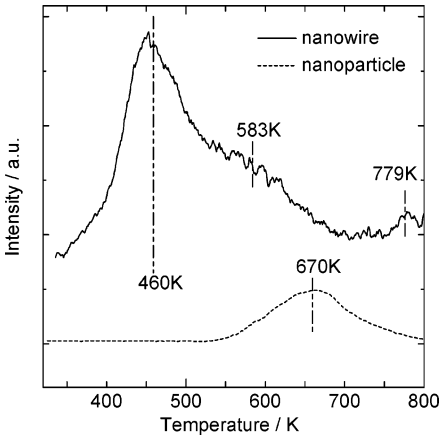

Figure 8. TPD profile of CO_2 absorbed on $SrCO_3$ nanowires and $SrCO_3$ nanoparticles.

3.3. Mechanism for Variation of Catalytic Activity with Nanostructure. The TPD profiles of CO_2 absorbed on nanowires and nanoparticles were studied to illustrate the different basic sites on these two catalysts, as shown in Figure 8. Nanowires showed three peaks at 460, 583, and 779 K, respectively, and the latter two were much weaker than the one at 460 K. These peaks can be attributed to three kinds of basic sites with different basicity. Different from nanowires, nanoparticles showed only one peak at 670 K, indicating that only one kind of strong basic site on the nanoparticle catalyst.

As shown Figure 4, the nanowire catalyst produced three products that existed at different temperature ranges, while the nanoparticle had only one main product at all temperatures. According to Figures 4 and 8, the basic sites were in agreement with the main product in both number and temperature.

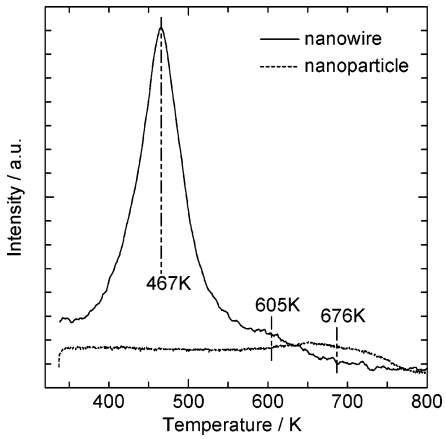

Figure 9. TPD profile of ethanol absorbed on $SrCO_3$ nanowires and $SrCO_3$ nanoparticles.

Therefore, it can be deduced that for nanowire the basic sites at 460, 583, and 779 K were related to the formation of CH_3CHO, CH_2O, and C_2H_4 and only the basic site at 670 K was related to the formation of CH_3CHO.

Ethanol-TPD over nanowires and nanoparticles was also studied. As shown in Figure 9, nanowires showed two desorption peaks at 467 and 605 K, respectively, and the former was much stronger than the latter. Different from nanowires, nanoparticles showed only one weak desorption peak at 676 K, whose intensity was comparable with the weak one of nanowires. These results were in agreement with Figure 8. In comparison of Figure 8 with Figure 3, it can be observed that the first desorption temperature of ethanol on nanowires was quite consistent with the ignition temperature. Furthermore, the second desorption temperature of the nanowires and the only desorption temperature of nanoparticles were in agreement with the temperatures at which the degradation of ethanol was about 65%. As shown in Figure 3, though nanowires had a much lower ignition temperature than that of nanoparticles, its total conversion temperature was almost the same as that of the nanoparticles. So the lower ignition temperature of the nanowires can be attributed to the active centers related to desorption at 467 K, while the total conversion of ethanol was mainly determined by the active center related to desorption over 600 K.

As mentioned above, the nanowires had a different distribution of active sites compared with that of nanoparticles. This may be because active sites were mainly determined by the crystal face. To decrease surface energy, particles tend to expose the most stable crystal face. However, since nanowires grew preferentially along the *c*-axis, the exposed crystal face was determined by the structure, and thus it may not be the most stable.

4. Conlusions

$SrCO_3$ nanowires had lower ignition temperatures and wider working temperature ranges than $SrCO_3$ nanoparticles, though nanowires had lower surface areas than those of nanoparticles. Besides, nanowires have different products than those of nanoparticles, and the products can change with reaction temperature, concentration, and flow rate. TPD analysis proved that differences of catalytic activity between nanowires and nanoparticles can be attributed to a different distribution of active sites with nanostructure, and the products correspond well with the enabled sites.

Acknowledgment. This work was partly supported by the Chinese National Science Foundation (20071021), the Trans-

Century Training Program Foundation for the Talents by the Ministry of Education, People's Republic of China, and the Excellent Young Teacher Program of the Ministry of Education, People's Republic of China.

References and Notes

(1) Spinicci, R.; Faticanti, M.; Marini, P.; De Rossi, S.; Porta, P. *J. Mol. Catal. A: Chem.* **2003**, *197*, 147. Soiron, S.; Aymard, L.; Rougier, A.; Tarascon, J. M. *Top. Catal.* **2001**, *16*, 391. Minico, S.; Scire, S.; Crisafulli, C.; Galvagno, S. *Appl. Catal. B* **2001**, *34*, 277.

(2) Marban, G.; Antuna, R.; Fuertes, A. B. *Appl. Catal. B* **2003**, *41*, 323. Dury, F.; Gaigneaux, E. M.; Ruiz, P. *Appl. Catal. A* **2003**, *242*, 187. Choudhary, T. V.; Banerjee, S.; Choudhary, V. R. *Appl. Catal. A* **2002**, *234*, 1.

(3) Cimino, S.; Colonna, S.; De Rossi, S.; Faticanti, M. L.; Pettiti, L. I.; Porta, P. *J. Catal.* **2002**, *205*, 309. Yang, L. F.; Shi, C. K.; He, X. E.; Cai, J. X. *Appl. Catal. B* **2002**, *38*, 117.

(4) Collins, P. G.; Bradley, K.; Ishigami, M.; Zettl, A. *Science* **2000**, *287*, 1801. Kong, J.; Franklin, N. R.; Zhou, C.; Chapline, M. G.; Peng, S.; Cho, K.; Dai, H. *Science* **2000**, *287*, 622.

(5) Cui, Y.; Wei, Q. Q.; Park, H. K.; Lieber, C. M. *Science* **2001**, *293*, 1289.

(6) Favier, F.; Walter, E. C.; Zach, M. P.; Benter, T.; Penner, R. M.; *Science* **2001**, *293*, 2227.

(7) Dickson, R. M.; Lyon, L. A. *J. Phys. Chem. B* **2000**, *104*, 6095. Lin, Y. M.; Cronin, S. B.; Ying, J. Y.; Dresselhaus, M. S.; Heremans, J. P. *Appl. Phys. Lett.* **2000**, *76*, 3944. Johnson, J. C.; Yan, H. Q.; Schaller, R. D.; Haber, L. H.; Saykally, R. J.; Yang, P. D. *J. Phys. Chem. B* **2001**, *105*, 11387.

(8) Shi, J. J.; Li, J. J.; Zhu, Y. F.; Wei, F.; Zhang, X. R. *Anal. Chim. Acta* **2002**, *466*, 69.

(9) Wang, L.; Zhu, Y. F. *Chem. Lett.* **2003**, *32*, 594.

(10) Qi, L. M.; Ma, J. M.; Cheng, H. M.; Zhao, Z. G. *J. Phys. Chem. B* **1997**, *101*, 3460.

(11) Xiong, G.; Zhi, Z. L.; Yang, X. J.; Lu, L. D.; Wang, X. *J. Mater. Sci. Lett.* **1997**, *16*, 1064.

(12) Church, J. S.; Cant, N. W. *Stud. Surf. Sci. Catal.* **1994**, *81*, 199.

(13) Shin, J. W.; Tornquist, W. J.; Korzeniewski, C.; Cherokee, S. *Surf. Sci.* **1996**, *364*, 122. Chen, G. L.; Sun, S. G.; Chen, S. P.; Zhou, Z. Y. *Electrochemistry* **2000**, *6*, 406.